Supplementary Information

Achieving Significant Thermal Conductivity Improvement via Constructing Vertically Arranged and Covalently Bonded Silicon Carbide Nanowires/Natural Rubber Composites

Shuaishuai Cheng[1], Xiaoyuan Duan[1], Xiaoqing Liu[1], Zhiyi Zhang[1,*], Dong An[1], Guizhe Zhao[1], Yaqing Liu[1,**]

[1]*Shanxi Key Laboratory of Nano-functional Composite Materials, North University of China, Taiyuan, 030051, China*

*Corresponding author.

** Corresponding author.

Tel: +86-351-3559669

E-mail addresses: zhiyzhang@sohu.com (Z. Zhang), lyq@nuc.edu.cn (Y. Liu).

1. The steady-state method of testing thermal conductivity

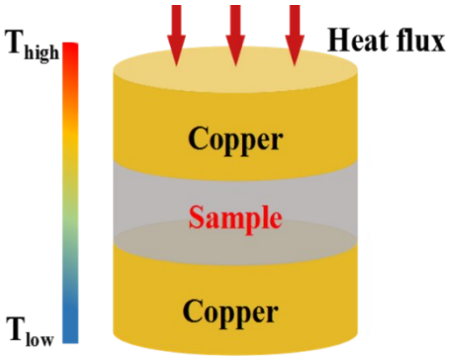

Figure. S1 Schematic diagram of thermal test principle

In the steady state method of testing, the sample to be tested is in a temperature field that does not vary with time, and when its internal thermal equilibrium is reached, the K can be obtained directly from Fourier's law by measuring the rate of heat flow per unit area of the sample, the temperature gradient in the direction of the heat flow and the geometry of the sample, etc. The Fourier's law formula is as follows.

$$K = -\frac{Q \cdot L}{\tau \cdot S \cdot \Delta T} = -\frac{W \cdot L}{S \cdot \Delta T} \quad \text{(S1)}$$

Where, W, L and S are the heat flux (W), sample thickness (m) and area (m^2), respectively. ΔT means temperature difference (℃).

The test equipment for thermal conductivity consists mainly of a cold and a hot copper column as shown in **Fig. S1**. The test sample is usually cut into a disc shape with a diameter of 20 mm and a thickness of about 2 mm. And the samples are placed between two columns with their temperatures of 70 ± 0.01°C and 30 ± 0.01°C, respectively, and with a pressure of 100 N between them. In addition, vacuum treatment is required before the test, and the vacuum level is about 133.32×10^{-3} Pa. By applying a known heat flux to create a certain temperature gradient, the K value is calculated based on the heat flux, sample thickness, area and temperature difference when the internal system reaches a steady state.

2. The morphology of SiCnw raw materials

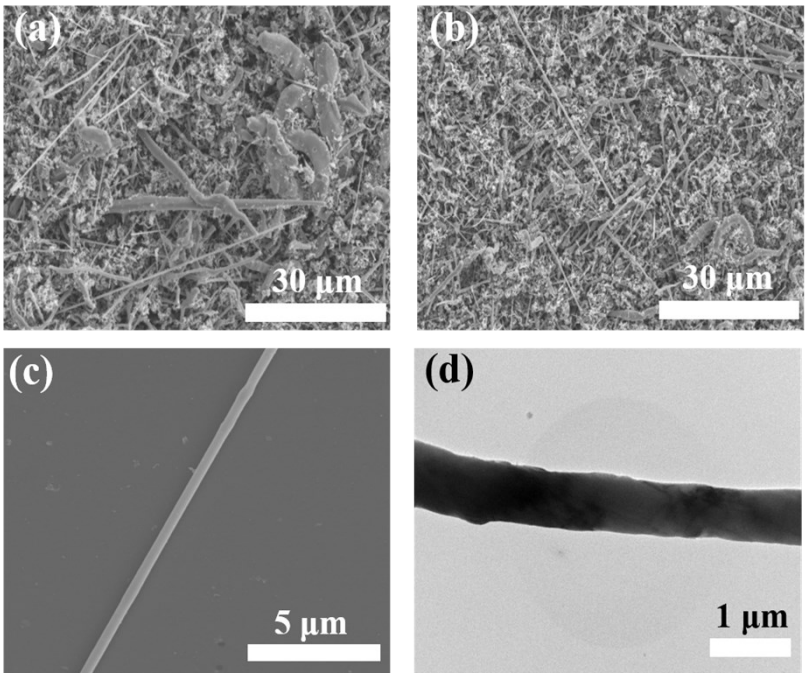

Figure S2. (a, b) SEM images of SiCnw before and after filtration. (c) SEM image of a single SiCnw. (d) TEM image of a single SiCnw.

Fig. S2a and **Fig. S2b** respectively showed the SEM images of raw SiCnw before and after filtration with a 45 μm metal screen. Compared with SiCnw before filtration, SiCnw after filtration had fewer large-diameter and irregular particles. It could be seen from **Fig. S2c** and **Fig. S2d** that the surface of SiCnw was relatively smooth and complete. And the SiCnw had a diameter of 400 nm-600 nm, a length of about 20 μm and an aspect ratio of about 20-30.

3. Energy Dispersive Spectroscopy (EDS) spectrum of SiCnw-SH

It showed that the SiCnw-SH surface treated with NaOH and silane coupling agent had a higher content of Si and C elements, and a small amount of S element was present. This indicated that a small amount of KH590 were grafted on the surface of SiCnw.

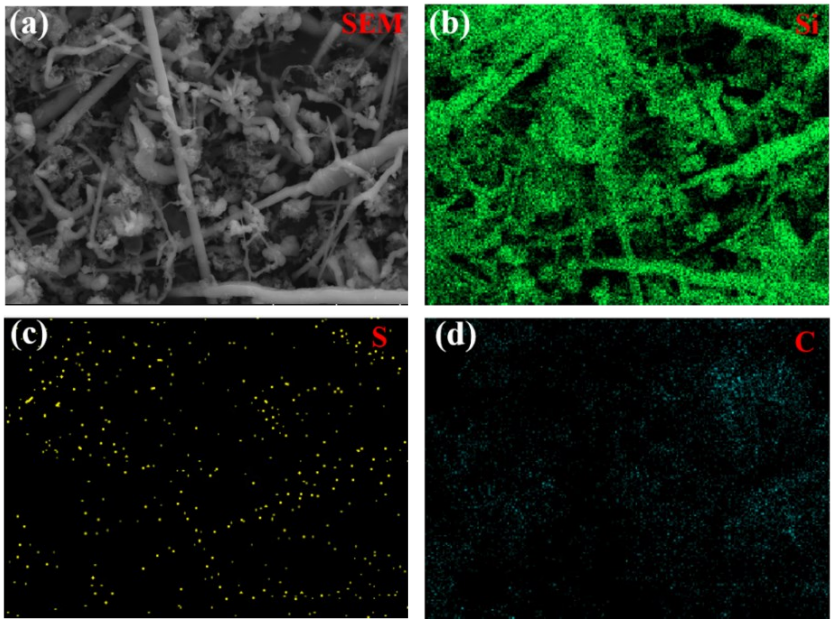

Figure S3. (a) SEM image and EDS images of SiCnw-SH: (b) Si element, (c) S element, (d) C element.

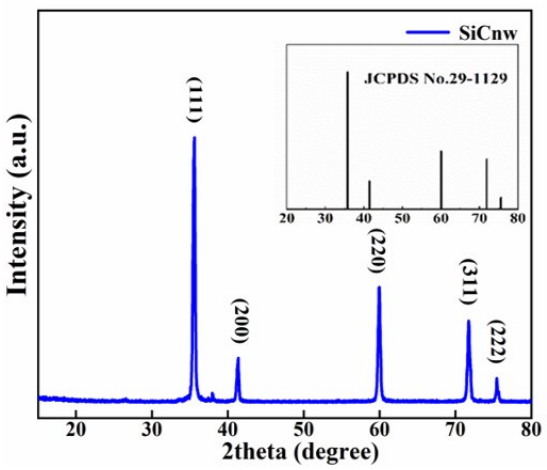

Figure S4. XRD spectrum of raw SiCnw.

From the XRD pattern of SiCnw **(Fig. S4)** was consistent with the crystal structure of its standard spectrum[1,2], indicating that SiCnw had a good crystal structure.

4. Element content ratio of SiCnw-SH in the testing of XPS

Table S1. Elemental composition of SiCnw-SH in XPS analysis.

Sample	C	Si	O	S
SiCnw	71.2	20.17	8.62	-
SiCnw-OH	68.54	17.66	13.8	-
SiCnw-SH	73.17	15.32	9.15	1.97

It could be seen from **Table S1** that compared to the raw SiCnw, the content of oxygen in SiCnw-OH after etching with NaOH increased. Combinated with **Fig. S3**, it showed that SiCnw was effectively etched by NaOH solution and grafted with a large number of -OH groups. In SiCnw-SH modified with KH590, the content of O and Si decreased, the content of C increased, and S appeared. There are two main reasons for this. On the one hand, the silane coupling agent reacted with the hydroxyl groups of SiCnw-OH surface, So the oxygen content was reduced; On the other hand, because the silane coupling agent was attached to the SiCnw surface, more

information about the surface silane coupling agent were received during the XPS testing, and the information about SiCnw were relatively less. Therefore, the chemical reaction between the silane coupling agent KH-590 and SiCnw-OH effectively occured.

5. Explain the interface interaction by low-field NMR

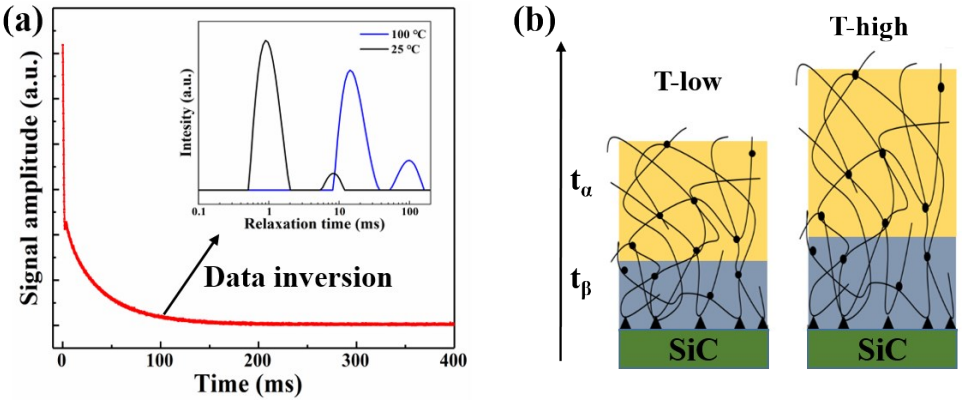

Figure S5. (a) The relaxation curve of rubber. (b) Schematic diagrams of bound rubber (α) and free rubber (β) in the rubber composites at low temperature (T-low) and high temperature (T-high).

To illustrate this kind of filler-matrix interaction force and the content of crosslinked rubber, LF-NMR was utilized to observe the compound rubber and vulcanized rubber[3–6]. The relaxation curve of rubber was obtained as shown in **Fig. S5a**. After data inversion, the relaxation peak of rubber was obtained. As shown in **Fig. S5b**, rubber adsorbed on the surface of the filler is the bound rubber, while rubber that does not undergo crosslinking reaction is the free rubber[7–9]. Among them, the bound rubber corresponds to the position of the α peak due to the shorter relaxation time, and the free rubber corresponds to the position of the β peak due to the longer relaxation time. The position of the α peak reflects the magnitude of filler-matrix interaction force, and the area of the α peak reflects the content of the binding rubber.

6. Method of converting mass parts to volume parts

For 3D f-SiCnw/NR composites, it was composed of NR matrix, rubber vulcanization aid and f-

SiCnw filler. When using the thermal conductivity model to fit the calculation, the mass fraction of the filler need to be converted into the volume fraction, which is converted by **Equation S2**.

$$V_f = \frac{\frac{m_f}{\rho_f}}{\frac{m_f}{\rho_f} + \frac{m_m}{\rho_m}} = \frac{W_f}{W_f + (1 - W_f)\frac{\rho_f}{\rho_m}} \tag{S2}$$

In the formula, V_f, m_f, ρ_f, and W_f respectively represent the volume fraction, mass, density and mass fraction of the filler, and ρ_f is 3.21 g/cm^3; m_m, ρ_m are the mass and density of the matrix, and ρ_m is 0.94 g/cm^3. **Table S2** shows the volume fraction corresponding to the mass fraction.

Table S2. The mass fraction of filler and the corresponding volume fraction.

Mass fraction (wt.%)	Volume fraction (vol.%)
0	0
5	1.52
10	3.15
15	4.91
20	6.82
25	8.89
30	11.15

7. Filler-matrix interaction of 3D f-SiCnw/NR

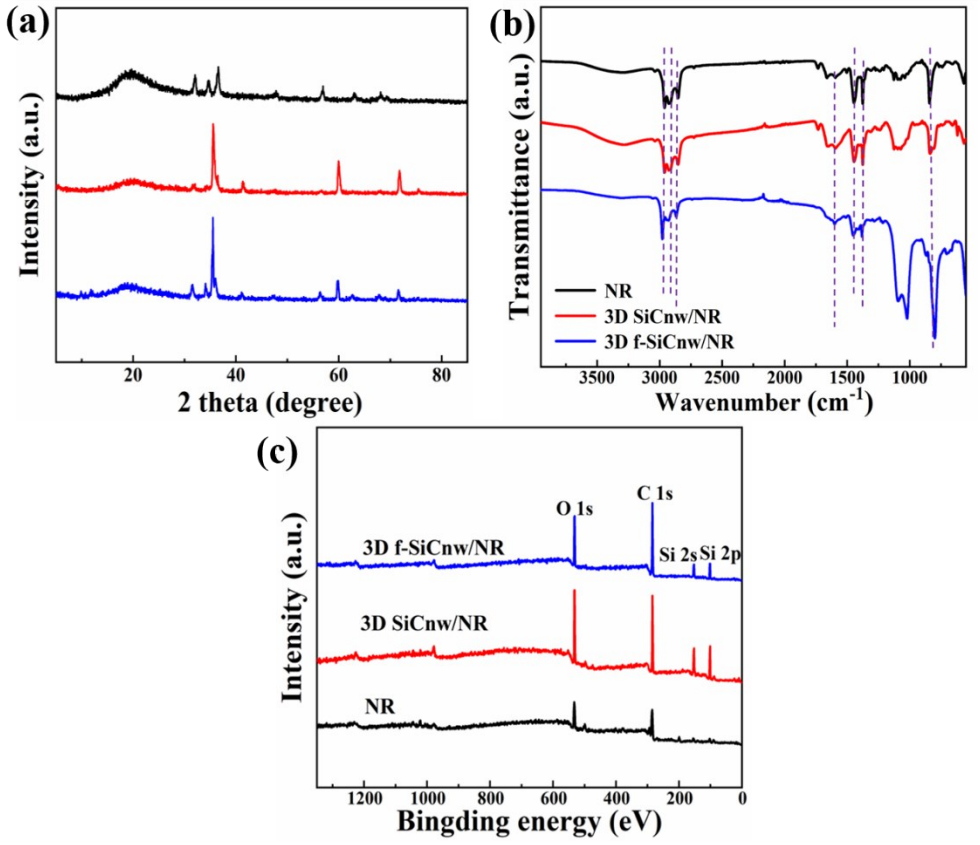

Figure S6. (a)XRD spectrum, (b)FTIR spectrum and (c)XPS spectrum of NR, 3D SiCnw/NR and 3D f-SiCnw/NR.

XPS, XRD, FTIR and other analytical methods had also been used in the process of characterizing the formation of chemical bonds between f-SiCnw and NR, and the element composition, lattice structure and chemical bonds of rubber composites had been tested.

It could be seen from **Fig. S6a** that when NR was vulcanized, a small amount of crystallization would appear. And when SiCnw were added to NR, there were five typical diffraction peaks of SiC in the XRD spectrum of the rubber composites. They all possessed strong diffraction peaks at 2θ values of 35.8°, 41.5°, 60.1°, 71.9° and 75.6°, corresponding to (111), (200), (220), (311) and (222) of face-centered cubic β-SiC, respectively (JCPDS No. 29-1129). This showed that after adding

SiCnw, the vulcanization process would not change the lattice structure of the filler.

From the FTIR spectrum (**Fig. S6b**), it could be seen that for NR, there were strong absorption peaks at seven positions, which were the asymmetric and symmetric stretching vibration peaks of $-CH_3$ at 2962 cm^{-1} and 1376 cm^{-1}, the asymmetric and symmetric stretching vibration absorption peaks of $-CH_2-$ at 2928 cm^{-1} and 2855 cm^{-1}, the stretching vibration peak of -CH=CH- at 1663 cm^{-1}, the antisymmetric vibration peak of $-CH_2-$ at 1449 cm^{-1}, and the out-of-plane deformation vibration absorption peak of C-H at -CH=CH- at 836 cm^{-1}. Compared with pure NR, the similar peaks were observed in 3D SiCnw/NR-25 and 3D f-SiCnw/NR-25, and more of them were the expression of NR peaks. This was because in actual experiments, a small amount of KH590 were used to modify SiCNw-OH, and the grafting rate was limited, resulting in a very small proportion of -SH functional groups in the fillers, so the proportion in the rubber composites was reflected especially few. Therefore, it was difficult to show the difference in structure through FTIR analysis.

Compared with pure NR, the Si element were observed in the XPS spectra (**Fig. S6c**) of 3D SiCnw/NR-25 and 3D f-SiCnw/NR-25, but its content was smaller than the actual content of Si, and the S element was not observed. This was mainly because the surface of SiCnw were wrapped with rubber macromolecules in rubber composites. However, XPS analysis belongs to the surface element analysis of test materials, and the depth that can be tested is about 10 nm. Therefore, the surface state change of SiCnw could not be completely detected under this condition.

8. Thermal Conductivity of NR, 3D SiCnw/NR and 3D f-SiCnw/NR with diffirent filler loading

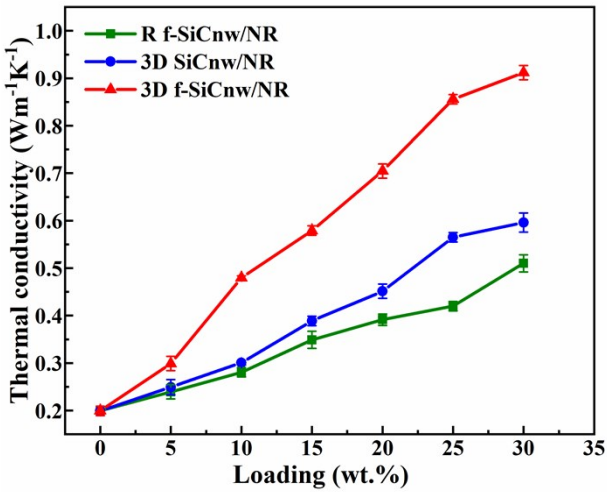

Figure S7. Thermal conductivity of R f-SiCnw/NR, 3D SiCnw/NR and 3D f-SiCnw/NR composites with different filler loadings.

As showed as in **Fig. S7,** the thermal conductivity of the composites gradually increased with the filler content increased, and the increase in the thermal conductivity of the 3D f-SiCnw/NR composites were particularly prominent. When the filler content were 30 wt.%, the thermal conductivity of the 3D f-SiCnw/NR composites reached 0.912 $Wm^{-1}K^{-1}$, but that of the 3D Sicnw/NR composites was only 0.614 $Wm^{-1}K^{-1}$, and R f-SiCnw/NR composites had the lowest thermal conductivity (0.501 $Wm^{-1}K^{-1}$). These showed that having a three-dimensional thermal conductivity network, and at the same time enhancing the filler-matrix interface interaction could significantly improve the thermal conductivity of the composites.

9. Volume resistivity of NR, 3D SiCnw/NR and 3D f-SiCnw/NR with diffirent filler loading

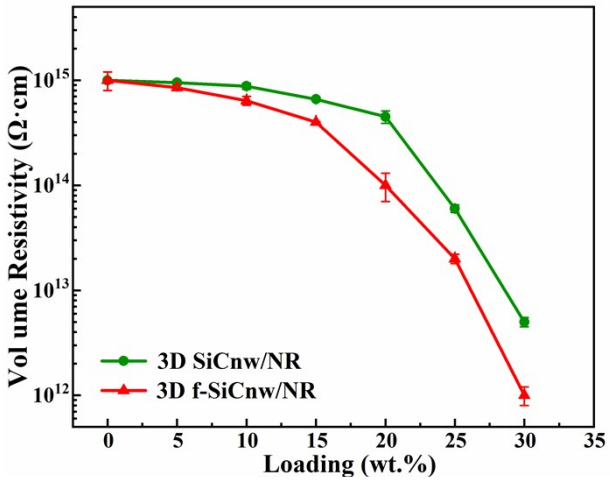

Figure S8. Volume resistivity of 3D SiCnw/NR and 3D f-SiCnw/NR composites with different filler loadings.

As showed as in **Fig. S8,** the volume resistivity of the composites gradually decreased with the filler content increased, and the decrease trend of the 3D f-SiCnw/NR composites were particularly prominent. When the filler content were 30 wt.%, the volume resistivity of the 3D f-SiCnw/NR composite was an order of magnitude lower than that of the 3D SiCnw/NR composite. However, the volume resistivity is still greater than 10^9 Ω·cm, so it can be regarded as an electrical insulating material.

References

[1] Y. Yao, X. Zeng, R. Sun, J.-B. Xu, C.-P. Wong, Highly Thermally Conductive Composite Papers Prepared Based on the Thought of Bioinspired Engineering, ACS Appl. Mater. Interfaces. 8 (2016) 15645–15653. https://doi.org/10.1021/acsami.6b04636.

[2] S. Paszkiewicz, I. Taraghi, A. Szymczyk, A. Huczko, M. Kurcz, B. Przybyszewski, R. Stanik, A. Linares, T.A. Ezquerra, Z. Rosłaniec, Electrically and thermally conductive thin elastic polymer foils containing SiC nanofibers, Composites Science and Technology. 146 (2017) 20–25. https://doi.org/10.1016/j.compscitech.2017.04.016.

[3] L.P. da Silva, L. Luetkrneyer, C.R.G. Furtado, M.I. Bruno Tavares, E.B.A.V. Pacheco, Characterization of pp/regenerated tire-rubber blends using proton spin-lattice relaxation time, POLYMER TESTING. 28 (2009) 53–56. https://doi.org/10.1016/j.polymertesting.2008.10.002.

[4] K. Singh, B. Bluemich, Compact low-field NMR spectroscopy and chemometrics: A tool box for quality control of raw rubber, POLYMER. 141 (2018) 154–165. https://doi.org/10.1016/j.polymer.2018.02.057.

[5] R. Zhang, T. Yan, B.-D. Lechner, K. Schroeter, Y. Liang, B. Li, F. Furtado, P. Sun, K. Saalwaechter, Heterogeneity, Segmental and Hydrogen Bond Dynamics, and Aging of Supramolecular Self-Healing Rubber, MACROMOLECULES. 46 (2013) 1841–1850. https://doi.org/10.1021/ma400019m.

[6] D. Besghini, M. Mauri, R. Simonutti, Time Domain NMR in Polymer Science: From the Laboratory to the Industry, APPLIED SCIENCES-BASEL. 9 (2019). https://doi.org/10.3390/app9091801.

[7] A.I. Medalia, Effective Degree of Immobilization of Rubber Occluded within Carbon Black

Aggregates, Rubber Chemistry and Technology. 45 (1972) 1171–1194. https://doi.org/10.5254/1.3544731.

[8] B. Omnès, S. Thuillier, P. Pilvin, Y. Grohens, S. Gillet, Effective properties of carbon black filled natural rubber: Experiments and modeling, Composites Part A: Applied Science and Manufacturing. 39 (2008) 1141–1149. https://doi.org/10.1016/j.compositesa.2008.04.003.

[9] Y. Yue, H. Zhang, Z. Zhang, Y. Chen, Polymer–filler interaction of fumed silica filled polydimethylsiloxane investigated by bound rubber, Composites Science and Technology. 86 (2013) 1–8. https://doi.org/10.1016/j.compscitech.2013.06.019.